A theoretical study of a nano-opto-mechanical sensor using a photonic crystal-cantilever cavity

2012 J. Opt. 14 075002

(http://iopscience.iop.org/2040-8986/14/7/075002)

J. Opt. **14** (2012) 075002 (8pp) doi:10.1088/2040-8978/14/7/075002

A theoretical study of a nano-opto-mechanical sensor using a photonic crystal-cantilever cavity

Depeng Mao[1], Peng Liu[1], Kai-Ming Ho[2] and Liang Dong[1]

[1] Department of Electrical and Computer Engineering, Iowa State University, Ames, IA 50011, USA
[2] US Department of Energy's Ames Laboratory and Department of Physics and Astronomy, Iowa State University, Ames, IA 50011, USA

E-mail: ldong@iastate.edu

Received 17 February 2012, accepted for publication 19 June 2012
Published 9 July 2012
Online at stacks.iop.org/JOpt/14/075002

Abstract
In this simulation study, integration of a nanocantilever inside a two-dimensional (2D) photonic crystal (PC) cavity resulted in a unique photonic crystal-cantilever cavity (PC^3), where the cantilever served as a tunable mechanical defect of the PC slab. Strong nano-opto-mechanical interactions between the cantilever and the defect-mode field inside the PC^3 gave rise to a high sensitivity of the resonance wavelength to surface stress-induced cantilever deflection. Mechanical and optical responses of the PC^3 to surface stress changes on the cantilever surface were studied by using a finite-element method (FEM) and a finite-difference time-domain (FDTD) method, respectively. Theoretical analysis revealed that the devised PC^3 sensor could resolve a conservative minimum surface stress at the level of $\sim$0.8 mN m^{-1}, representing state-of-the-art cantilever sensor performance. Also, the PC^3 sensor design used an ultracompact structure with an on-chip optical length of only several microns, while a conventional reflected laser beam detection scheme requires a $\sim$1 m long free-space optical path.

Keywords: photonic crystals, optical cavity, cantilever, sensor

(Some figures may appear in colour only in the online journal)

1. Introduction

Label-free detection of chemical and biological species is a rapidly growing research area with wide applications ranging from clinical diagnostics, environmental monitoring, explosive detection, and biological research [1]. Many label-free optical sensor platforms have been established such as surface plasmon resonance [2], interferometry [3], evanescent waveguides [4], Bragg reflectors [5], photonic nanocavity laser sensors [6], and diffractive gratings [7]. These sensor techniques often require collimated readout optical beams and hence a relatively large sensing area [8]. To solve this problem, researchers developed nanophotonic biochemical sensors based on a 2D PC resonant cavity capable of confining light to an ultrasmall volume [8–11]. Generally, a simple PC cavity is formed by introducing a defect to a perfect PC and the resonance wavelength of the cavity is sensitive to a change in its effective refractive index Δn [11]. However, biochemical binding or molecular adsorption to the surface of a PC cavity produced only an ultrathin molecule coating, and thus, caused a small change in Δn, and thus, a limited resonance wavelength shift of the conventional PC cavity sensor [8, 11].

A competing non-optical label-free biochemical sensor approach utilizes micro/nano-sized mechanical cantilevers. The sensing mechanism involves changing surface stress on the surface of a cantilever due to specific molecular binding or adsorption. The change in surface stress can cause the cantilever to bend. To detect the deflection of the cantilever, a laser beam is focused on the tip of the cantilever and a

position-sensitive detector (PSD) detects a position shift of the reflected beam [12]. This conventional method provides tremendous sensitivity and the state-of-the-art surface stress detection limit is ∼1 mN m^{-1}. However, it requires a large optical distance (∼1 m) in free space to amplify the cantilever deflection [13], hindering further miniaturization of the sensor system.

We point out that in order for the conventional PC cavity sensors to achieve high sensitivity, an amplification mechanism is desired to amplify the molecular binding- or adsorption-induced index change, while maintaining the features of small sensing area and short optical path. On the other hand, in order for the conventional cantilever sensors to reduce system dimensions, a compact deflection detection scheme is needed to interrogate cantilever deflections, while maintaining the high sensitivity. Recently, nano-opto-mechanical interactions between mechanical structures and PCs have attracted much attention for a range of device applications [14–23]. Iwamoto and *et al* developed a PC line-defect waveguide integrated with an integrated moveable dielectric plate for a tunable optical switch [14]. The movement of the plate towards the PC surface modulated the transmittance of the PC waveguide. Takahata *et al* reported that the transmittance of a PC waveguide could be controlled by moving the height difference between the PC slab and silicon rods [15]. Also, Abdulla *et al* developed another interesting tunable PC waveguide. The PC waveguide was integrated with a MEMS cantilever actuator for electro-opto-mechanical modulation of light transmission [16]. Besides, tuning the resonance of a PC cavity has been reported with a scanning probe microscope (SPM) probe and an atomic force microscope (AFM) cantilever [22]. Researchers demonstrated that the switching and tuning of a PC cavity resonance was achievable by approaching a mechanical tip to the cavity [23]. Overall, these tunable optical devices were developed by taking benefits from the strong mechanical–optical interactions on a 2D PC platform and their optical properties were mechanically tuned by position control actuators. Despite these developments, to the best of our knowledge, there are few reports in the literature of nano-opto-mechanical sensors using remarkable mechanical–optical interactions on a 2D PC platform.

In this paper, we devised a novel nano-opto-mechanical sensor that had a compact device structure comparable to the conventional PC cavity sensors, and sensitivity higher than or at least comparable to that of the conventional cantilever sensors. The basic approach was to integrate a nanocantilever inside a PC cavity to form a unique PC^3. By matching the characteristic size of the defect mode of the PC cavity by the dimensions of the cantilever, the surface stress-induced cantilever bending would significantly influence the defect-mode field inside the cavity, resulting in a massive change in effective index of the cavity, and thus, a large shift in its resonance wavelength.

2. Architecture and design of PC^3

Figures 1(a) and (b) show the schematic for the PC^3 sensor. In this theoretical study, a silicon-on-insulator (SOI) wafer

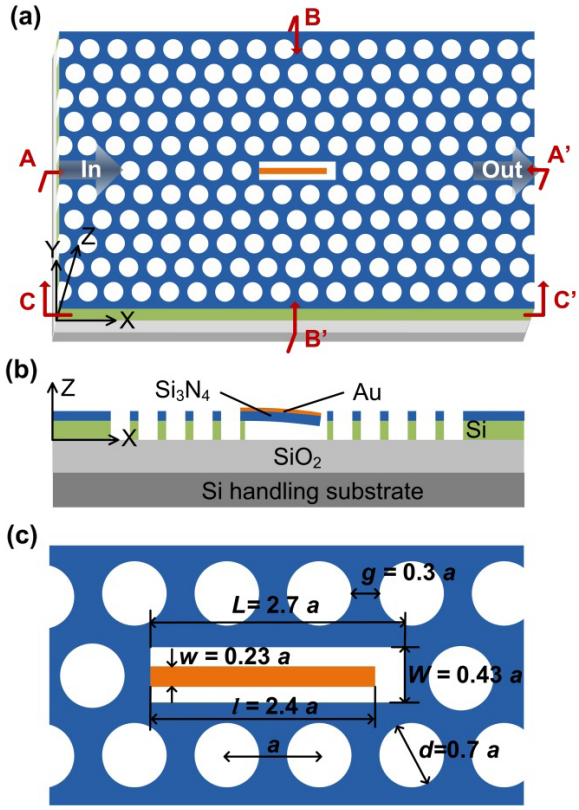

Figure 1. Schematic for the devised PC^3 device. (a) Top view. (b) Cross-sectional view. (c) Magnified view of the PC^3 region to show structural parameters.

served as the substrate of the device. A Si_3N_4 thin film was deposited on the top silicon (Si) layer of the SOI wafer. A PC was formed by creating periodic holes in the Si_3N_4/Si composite membrane. An ultrathin gold (Au) layer was formed on the top surface of a cantilever at the center of the PC. Generally, the Au layer allows facilitating surface chemical functionalization (e.g., Au–thiol bond) with probe molecules for specific sensing purpose. The Au/Si_3N_4 cantilever was suspended in a rectangular hosting hole and centered between two identical PC Bragg reflectors in the Γ–M direction of triangular coordinates. The input and output waveguides were formed by missing holes on two ends of the reflectors.

To obtain an appropriate photonic bandgap (PBG) for transverse-electric (TE)-like modes, the diameter of the perfect holes of the Si_3N_4/Si PC was chosen to be $d = 0.7a$, where a is the lattice constant of the PC (figure 1(c)). To study the influence of the Si_3N_4 layer on the optical and mechanical properties of the PC^3, the thickness of the Si_3N_4 layer $t_{Si_3N_4}$ varied from $0.11a$ to $0.23a$ and $0.34a$. The thickness of Au was fixed at 20 nm, which generally allows efficient immobilization of probe molecules on its surface. The Drude model was used for Au in the simulation [24]. The length and width of the cantilever were set to be $l = 2.4a$ and $w = 0.23a$, respectively. The length and width of the central hosting hole were set to be $L = 2.7a$ and $W = 0.43a$, respectively. The thickness of the top Si layer and oxide layer were set to be $0.8a$ and $1.38a$, respectively. As we will see later, this

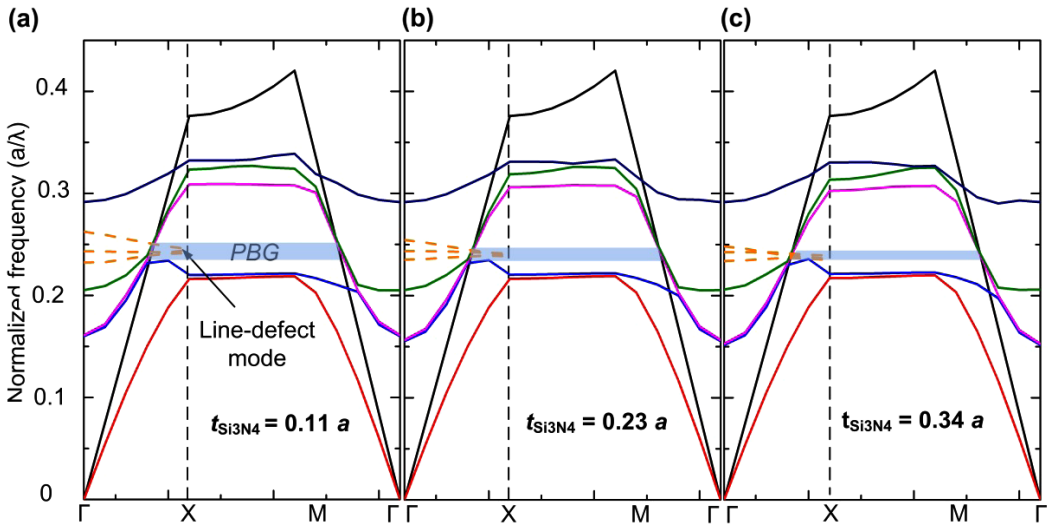

Figure 2. (a)–(c) Band diagrams of TE-like modes for the perfect Si/Si_3N_4 PC structure and dispersion curves of line-defect modes (orange dashed lines) along the Γ–X direction for different $t_{Si_3N_4}$: 0.11a (a), 0.23a (b), and 0.34a (c).

design allowed for the formation of the PC^3. Note that the minimum gap between two regular holes was 0.3a, which was larger than the width of the cantilever. This will allow us to release the cantilever without etching through the top silicon layer between two regular holes during device fabrication in the future. In the following simulations, the device was considered to work in an aqueous environment (here, water, refractive index 1.33) for the purpose of biochemical sensing, and thus, all holes in the device were filled with water. The dielectric constant of Si, Si_3N_4, and SiO_2 was 11.68, 7.50, and 3.90, respectively.

Figure 2 shows the three band diagrams for TE-like modes of the perfect Si/Si_3N_4 PC with $t_{Si_3N_4} = 0.11a$, 0.23a, and 0.34a. Since all structural parameters of the PC were proportional to the lattice constant a, a three-dimensional (3D) plane-wave transfer matrix method with periodic boundary conditions was used. The SiO_2 layer was included in the simulation structure. Rectangular coordinates were used because the Γ–X direction in rectangular coordinates is generally equivalent to the Γ–M direction in triangular coordinates. No PBG for TM-like modes was found beneath the light cone. As $t_{Si_3N_4}$ increased from 0.11a to 0.23a to 0.34a, the normalized frequency gap for TE-like modes decreased from 0.0152 to 0.0083 to 0.0031, and thus, the corresponding central frequency red shifted from 0.2418 to 0.2389 to 0.2374. By choosing $a = 435$ nm for all of the three cases, the central wavelength of the PBG was near 1815 nm. Therefore, $t_{Si_3N_4} = 50$, 100, and 150 nm were used in the following discussions. Also, we found several guided modes of a line-defect waveguide in the PBG structure along the Γ–X direction (orange dashed lines in figure 2). This result indicated the possibility of employing these guided modes to couple the light into and out of the PC^3 device.

3. Mechanical response of cantilever to surface stress

The deflections of the cantilever under different applied surface stress were simulated by using the software ANSYS (Ansys Inc.) based on a FEM method. The cantilever was modeled with eight-node 3D brick elements (SOLID 186). The mechanical response of the cantilever for an applied surface stress was calculated under a static stress loading condition. It is known that generally, the initial surface stress on a micro/nanomachined cantilever is dependent on the methods and conditions used for depositing the thin films of the cantilever. Here, in this simulation, for demonstration purposes, Young's modulus of the Si_3N_4 and Au film was set to be 80 and 210 GPa, respectively. Poisson's ratio of the Si_3N_4 and Au film was fixed at 0.42 and 0.24, respectively [25, 26]. The resulting initial surface stress on the top surface of the cantilever appeared compressive. Thus, the cantilever initially bent downward into the central hosting hole. As a tensile (compressive) stress (caused by molecular binding/adsorption during sensing) to the top surface of the cantilever, the cantilever bent upward (downward) from its initial bending condition. As an example, figure 3(b) shows the simulated bending profiles of the cantilever under three different applied surface tensions for $t_{Si_3N_4} = 100$ nm. As we will see later, the bending of the cantilever could cause a shift of the resonance wavelength of the PC^3. Figure 3(a) shows that the vertical deflection at the tip of the cantilever Δz was linear to an applied surface stress. The thicker the Si_3N_4 layer used, the lower the displacement of the cantilever observed. By fitting the data with a linear function, the changing rate of deflection with increasing surface stress was found to be 3.32, 1.40, and 0.79 nm $(mN/m)^{-1}$ for $t_{Si_3N_4} = 50$, 100, and 150 nm, respectively.

4. Optical responses of PC^3 to mechanical perturbations

To investigate how the mechanical bending of the cantilever influenced the resonance shift of the PC^3, 3D electromagnetic simulations were performed by using the FDTD method with the freeware package MEEP [27]. The computing region covered a 300 nm thick top water layer, a 5 nm molecule

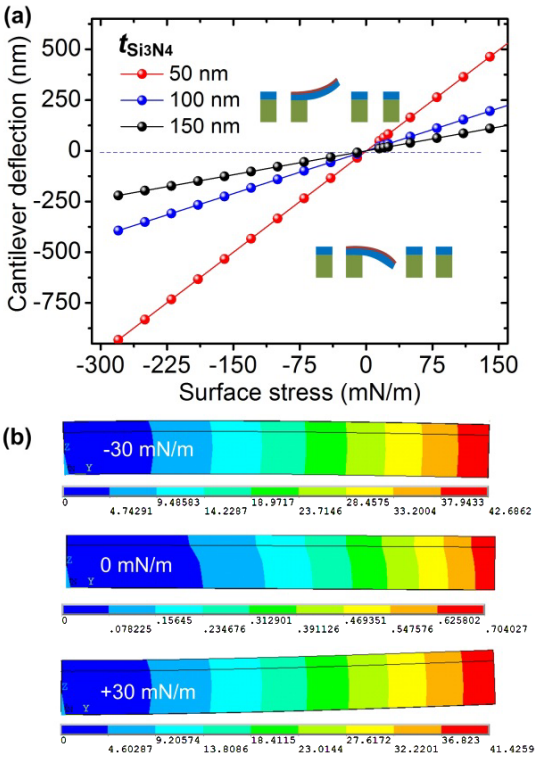

Figure 3. (a) Vertical displacement at the tip of the cantilever as a function of an applied surface tension. (b) Bending profiles of the cantilever ($t_{Si_3N_4} = 100$ nm) by the surface tension of -30 (compressive), 0, and $+30$ mN m^{-1} (tensile).

layer (refractive index: ∼1.4), the Au, the Si_3N_4, the top Si, and the SiO_2 layers, from top to bottom. Generally, molecular binding- or adsorption-induced coating on a surface is only a fraction of a nanometer or several nanometers thick. Considering the grid resolution of 2.5 nm, we chose 5 nm (a relatively large thickness) for the molecule coating layer covering simulation grids in the vertical direction. 150 nm thick perfectly matched layers (PMLs) were applied at the boundaries of the entire computing region. 17 periods of the photonic lattice in the Γ–M direction and 11 periods in the M–K direction were covered. The handling substrate of the SOI wafer was excluded because as we can see later, the mode profiles hardly reached the substrate through the SiO_2 layer. A TE-polarized pulse line source with a Gaussian frequency distribution was placed vertically along the Z direction and offset by 20 nm from the spatial center of the hosting air hole. This line source had the same height as the top Si layer. The resonance wavelength and Q factor of the PC^3 were computed according to Harminv [28]. To record the mode profiles, a continuous-wave line source at resonance was used.

Figure 4 shows the resonance mode profiles of the PC^3 under different bending conditions of the cantilever with $t_{Si_3N_4} = 50$ nm (figure 4(a)), 100 nm (figure 4(b)), and 150 nm (figure 4(c)). Here, the mode profiles were taken after propagation over a distance of 1000 wavelengths. The defect-mode field distributions demonstrated the capability of the PC^3 to confine the mode fields in all three dimensions. In the case of $t_{Si_3N_4} = 100$ nm (figure 4(b)), when the vertical displacement at the tip of the cantilever was $\Delta z = -320$ nm, -100 nm, 0, and $+100$ nm from the top surface of the slab, the resonance frequency of the cavity was 0.2370, 0.2392, 0.2397, and 0.2401 c/a, and thus, the resonance wavelength was 1838.8, 1818.2, 1814.4, and 1812.5 nm, respectively. For $t_{Si_3N_4} = 100$ nm, the Q factor of the cavity was 113.7, 125.6, 145.2, and 117.8 when $\Delta z = -320$, -100, 0, and $+100$ nm, respectively. We note that the Q factor was relatively low and slightly degraded as the cantilever bent downward inside the hosting hole. The explanation for the slight Q degradation is as follows: the Q factor in the planar direction (X–Y plane) was determined mainly by the geometry and location of the hosting hole, while only slightly by the bending location of the cantilever inside the hosting hole. It is noteworthy that the defect-mode field leakage into the SiO_2 layer was limited. This allowed us to neglect the Si handling substrate in these simulations. When $t_{Si_3N_4} = 50$ (figure 4(a)) and 150 nm (figure 4(c)), the PC^3 attained the capability of localizing the defect-mode field as the cantilever bent inside and outside the cavity.

Since an incident light near the resonance wavelength was able to tunnel through the PC^3, the detection of a surface stress change on the cantilever surface would be possible, by detecting the peak wavelength (or the resonance wavelength) shift in the transmission spectrum at the output of the device. Here, TE-polarized incidence of a broadband light was incident laterally on the device in the Γ–M direction. Figures 5(a)–(c) show that the transmission peak red shifted when the cantilever bent downward into the hosting hole over the entire thickness of the slab from 0 to -320 nm, and blue shifted when it bent upward out of the hosting hole up to $+150$ nm. Interestingly, the resonance wavelength shifted more rapidly when the cantilever bent downward than it did when the cantilever bent upward. As the defect-mode field strength outside the slab was much lower than that inside the slab (figure 4), the nano-opto-mechanical interaction between the cantilever and the defect-mode field was relatively weak when the cantilever was outside the slab. However, when the cantilever bent inside the hosting hole, this interaction became more intensive, and thus, the mode field became more sensitive to the deflections of the cantilever.

Although the molecule coating was already considered in the previous simulations (figures 4 and 5), it was interesting to examine the influence of the molecule coating thickness t_{mol} on the optical properties of the PC^3. We conducted the simulation for three different thicknesses of $t_{mol} = 0$, 5, and 7.5 nm in figure 6. Since we intended to have the minimum feature size of the simulation structure (here, t_{mol}) to cover at least two simulation grids (the grid resolution used was 2.5 nm), no simulation was conducted for $0 < t_{mol} < 5$ nm. Figure 6(b) compares the mode profiles and resonance wavelengths between the PC cavities with different t_{mol}. To simplify the discussion, we assumed that each cantilever bent downward from the horizontal plane ($\Delta z = 0$) to the same low level at $\Delta z = -320$ nm. We found in figures 6(b)–(d) that the mode profiles of the three cavities were almost the same. As shown in figure 6(a), their resonance wavelength slightly red shifted as t_{mol} increased from 0 to 7.5 nm. Specifically,

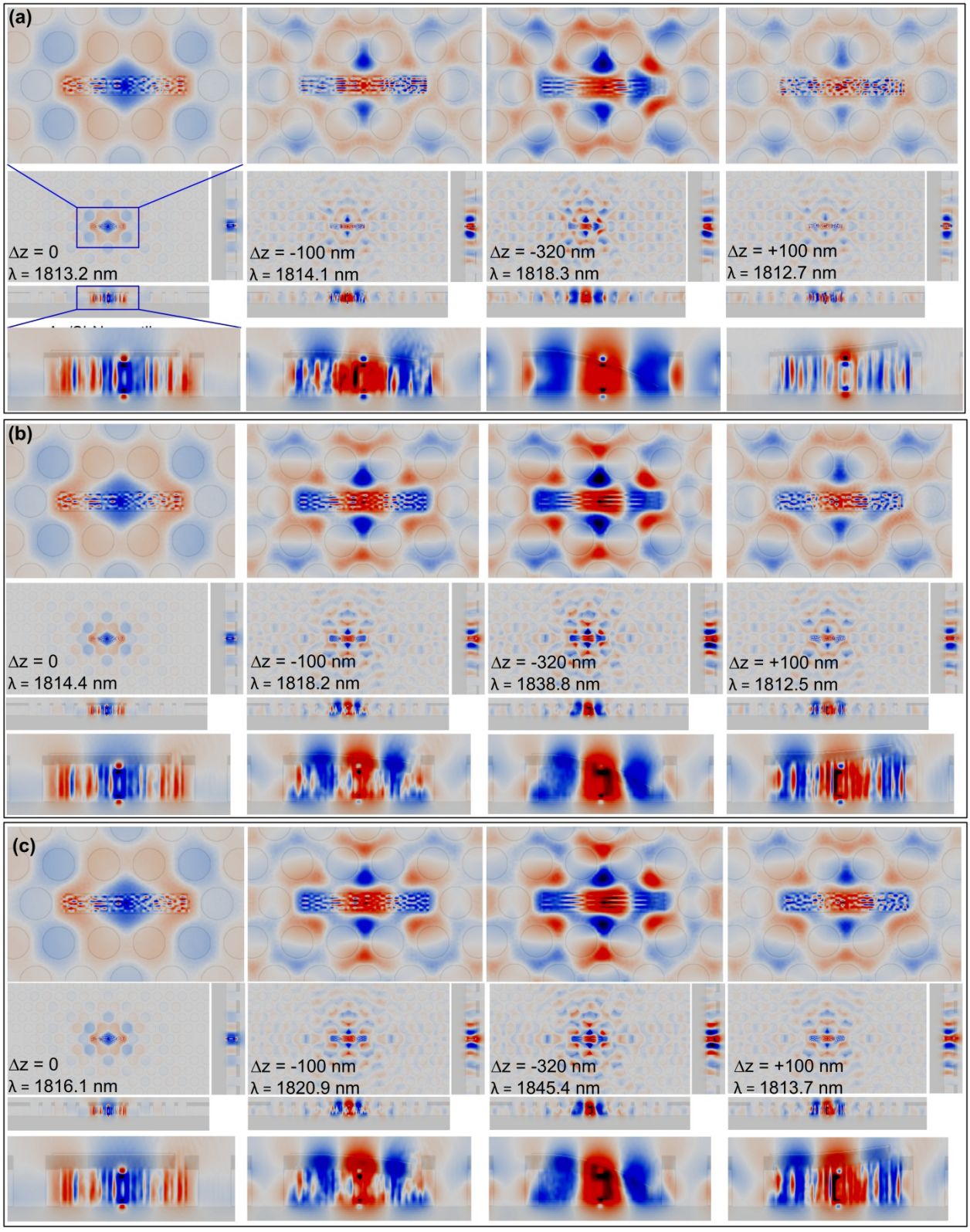

Figure 4. Electric field (amplitude) distributions at the resonance mode of the PC^3 for $t_{Si_3N_4} = 50$ nm (a), 100 nm (b), and 150 nm (c). In the middle row of each panel, the four images from left to right show the field distributions when $\Delta z = 0$, -100, -320, and $+100$ nm, respectively, and each image contains three smaller images showing the field distributions in the plane of *X*–*Y*, *Y*–*Z*, and *X*–*Z*, at the cross section of C–C′, B–B′, and A–A′, respectively (see figure 1). In the bottom and top rows of each panel, the images from left to right display the magnified field distributions around the cavity at the A–A′ and C–C′ cross sections. The resonance wavelength λ for each device structure is also given in the figure.

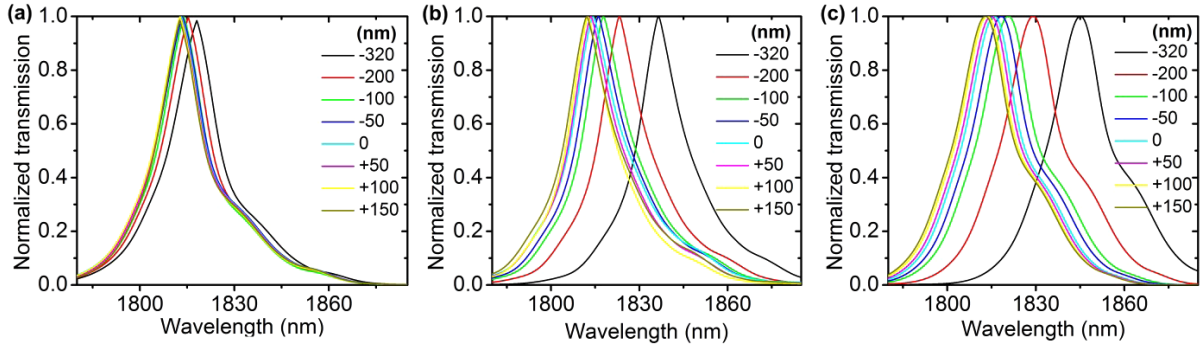

Figure 5. Normalized transmission of the PC^3 under different bending conditions of the cantilever for $t_{Si_3N_4} = 50$ nm (a), 100 nm (b), and 150 nm (c).

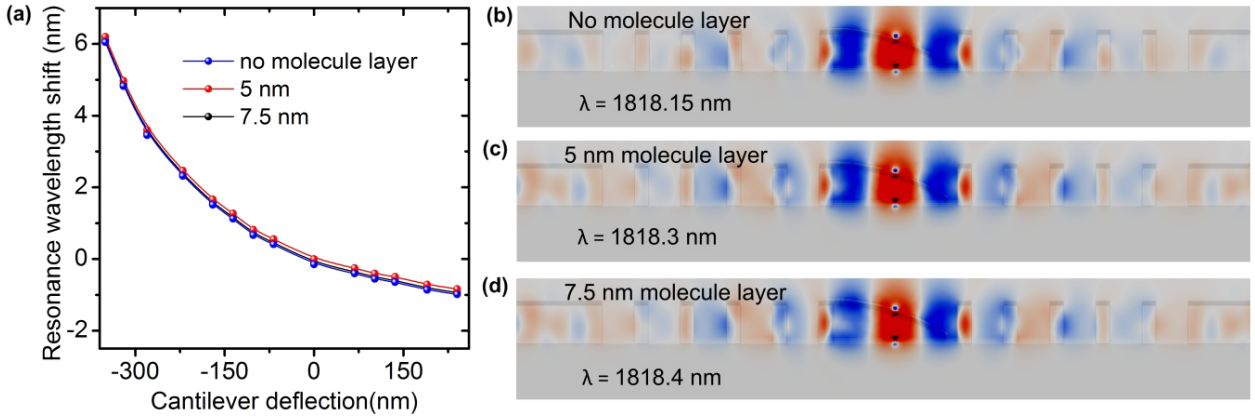

Figure 6. (a) Resonance wavelength shift of the PC^3 as a function of a deflection of the cantilever ($t_{Si_3N_4} = 50$ nm) for $t_{mol} = 0$, 5 nm, and 7.5 nm. (b)–(d) Electric field (amplitude) distribution at the resonance mode of the PC^3 in the X–Z plane at the A–A′ cross section (see figure 1(a)) when $t_{mol} = 0$ (b), 5 nm (c), and 7.5 nm (d).

at $t_{mol} = 0$, 5, and 7.5 nm, the resonance wavelength was 1818.15, 1818.3 and 1818.4, respectively. Obviously, the differences ($\leq$0.25 nm) were considered negligibly small (compared to the total resonance wavelength shift of $\sim$7 nm as the cantilever bent from 0 to -320 nm). Therefore, the optical properties of the cavity were little changed by the variation in cantilever thickness (due to the contact of an analyte with the cantilever's top surface).

By combining the mechanical response of the cantilever to an applied surface stress (figure 3) and the optical response of the PC^3 to a mechanical bending of the cantilever (figure 7(a)), we obtained the resonance response of the PC^3 to an applied surface stress shown in figure 7(b). The thin cantilever deflected easily, but, due to the insufficient interaction between the thin cantilever and the mode field, the resonance wavelength shift with $t_{Si_3N_4} = 50$ nm was a little less sensitive to a surface stress change than that with $t_{Si_3N_4} =$ 100 nm (see the slopes of the plots). On the other hand, the thick cantilever deflected with more difficultly than the thin one under the same surface stress condition. The resonance wavelength shift with $t_{Si_3N_4} = 150$ nm changed more slowly with varying surface stress than that with $t_{Si_3N_4} = 100$ nm. Therefore, we found that when $t_{Si_3N_4} = 100$ nm the resonance shift changed most rapidly with changing surface stress. We used the mean surface stress sensitivity of resonance shift $S_{\Delta\lambda\to\tau}$ to evaluate the influence of $t_{Si_3N_4}$ on the optical properties of the PC^3. Specifically, for $t_{Si_3N_4} = 100$ nm, $S_{\Delta\lambda\to\tau}$ reached a maximum value of 0.13 nm (mN/m)$^{-1}$ when the cantilever bent inside the slab (figure 7(c)), while only 0.021 nm (mN/m)$^{-1}$ when bent outside the slab. By adjusting the material properties, processing conditions and structural geometries of the cantilever, the initial bending of the cantilever can be well controlled [29, 30]. Therefore, it is possible to have all surface stress-induced cantilever bending activities occur inside the slab, allowing us to obtain high sensitivity of the PC^3 sensor to surface stress.

Generally, the detection resolution of a conventional optical spectrometer is $\sim$0.1 nm (conservatively). Thus, theoretically, the sensor can resolve a surface stress of $\sim$0.77 mN m^{-1}, which is higher than that of the state-of-the-art detection limit ($\sim$1 mN m^{-1}) of the cantilever sensors [12]. For a practical example, hybridization of the 12-mer oligonucleotides can produce a compressive surface stress of 5 mN m^{-1} in a liquid environment [31]. Theoretically, when using the devised PC^3 scheme, we will be able to easily observe the resonance wavelength shift of $\sim$0.65 nm on a conventional spectrometer. Also, presently the lowest detectable concentration of non-amplified RNA from a cell is 10 pM, which is limited by the surface stress sensitivity (1 mN m^{-1}) of a conventional cantilever

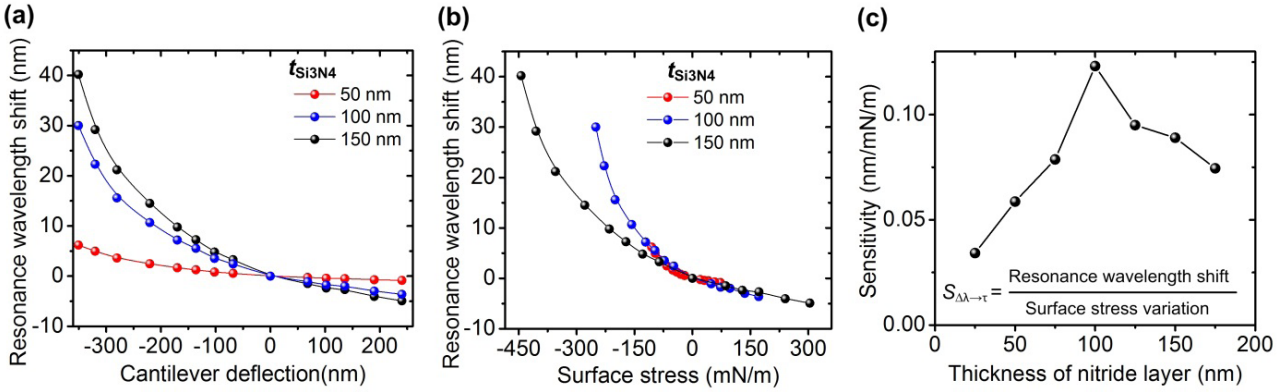

Figure 7. (a) Resonance wavelength shift of the PC^3 as a function of cantilever bending. (b) Resonance wavelength shift of the PC^3 as a function of an applied surface stress. (c) Mean surface stress sensitivity as a function of $t_{Si_3N_4}$ when the cantilever bent inside the slab.

sensor [32]. Therefore, the present PC^3 sensor technology possibly can push the lowest detectable concentration of non-amplified RNA down to only several pM, which will be comparable with conventional gene-chip technologies with fluorescent probes.

As mentioned early, the current standard for the cantilever-based surface stress detection is as high as $\sim$1 mN m^{-1}. However, to achieve that sensitivity, the laser beam reflected by the cantilever needs to propagate in free space for $\sim$1 m to obtain a sufficient deviation of the beam spot from the center of the PSD. In contrast, the present PC^3 technology allows for a much more compact sensor structure. The on-chip optical length of the sensor is several micrometers. The output light of the sensor potentially can be coupled to an external fiber at the end of the on-chip output waveguide and detected by a handheld spectrometer for the readout. Therefore, the present sensor has the potential to eliminate the need for a long free-space light traveling distance. Also, compared to many miniaturization efforts on integrating a piezoresistive or piezoelectric deflection detection circuit with a cantilever sensor [33, 34], the present sensor needs relatively less special care of isolating on-chip detection electronics from surrounding fluidic and chemical environments.

5. Conclusion

In this simulation paper, we designed a nano-opto-mechanical biochemical sensor using a cantilever-in-PC cavity structure. The surface stress-induced bending of the nanocantilever modulated the effective refractive index, and thus, the resonance wavelength, of the cavity. The theoretical analysis showed that the sensor could resolve a minimum surface stress of $\sim$0.8 mN m^{-1}, representing the state-of-the-art cantilever sensor performance. The PC^3 sensor was also designed with an on-chip optical length of only several microns. This nano-opto-mechanical sensor scheme could shed light on biochemical sensors where surface stress develops on the cantilever surface due to the probe–target molecule interaction. The PC^3 could also be useful for understanding the coupled interactions between nanomechanics and nanophotonics [35, 36].

Acknowledgments

This work is supported the NSF under CAREER Award (0954765), the US DOE's Basic Energy Sciences Office through the Ames Laboratory, and China Scholarship Council.

References

[1] Fan X, White I M, Shopoua S I, Zhu H, Suter J D and Sun Y 2008 Sensitive optical biosensors for unlabeled targets: a review *Anal. Chim. Acta* **620** 8–26
[2] Homola J 2008 Surface plasmon resonance sensors for detection of chemical and biological species *Chem. Rev.* **108** 462–93
[3] Ymeti A, Kanger J S, Greve J, Lambeck P V, Wijn R and Heideman R G 2003 Realization of a multichannel integrated Young interferometer chemical sensor *Appl. Opt.* **42** 5649–60
[4] Skivesen N, Tetu A, Kristensen M, Kjems J, Frandsen L H and Borel P I 2007 Photonic-crystal waveguide biosensor *Opt. Express* **15** 3169–76
[5] Guo Y, Divin C, Myc A, Terry F L, Baker J R, Norris T B and Ye J Y 2008 Sensitive molecular binding assay using a photonic crystal structure in total internal reflection *Opt. Express* **16** 11741–9
[6] Loncar M, Scherer A and Qiu Y 2003 Photonic crystal laser sources for chemical detection *Appl. Phys. Lett.* **82** 4648–50
[7] Cunningham B, Lin B, Qiu J, Li P, Pepper J and Hugh B 2002 A plastic colorimetric resonant optical biosensor for multiparallel detection of label-free biochemical interactions *Sensors Actuators* B **85** 219–26
[8] Lee M K and Fauchet P M 2007 Two-dimensional silicon photonic crystal based biosensing platform for protein detection *Opt. Express* **15** 4530–5
[9] Foresi J S, Villeneuve P R, Ferrera J, Thoen E R, Steinmeyer G, Fan S, Joannopoulos J D, Kimerling L C, Smith H I and Ippen E P 1997 Photonic-bandgap microcavities in optical waveguides *Nature* **390** 143–5
[10] Lee M R and Fauchet P M 2007 Nanoscale microcavity sensor for single particle detection *Opt. Lett.* **32** 3284–6
[11] Kang C and Weiss S M 2008 Photonic crystal with multiple-hole defect for sensor applications *Opt. Express* **16** 18188–93
[12] Fritz J 2008 Cantilever biosensors *Analyst* **133** 855–63
[13] Carrascosa L G, Moreno M, Alvarez M and Lechuga L 2006 Nanomechanical biosensors: a new sensing tool *TRAC Trends Anal. Chem.* **25** 196–206

[14] Iwamoto S, Ishida S, Arakawa Y, Tokushima M, Gomyo A, Yamada H, Higo A, Toshiyoshi H and Fujita H 2006 Observation of micromechanically controlled tuning of photonic crystal line-defect waveguide *Appl. Phys. Lett.* **88** 011104

[15] Takahata T, Matsumoto K and Shimoyama I 2010 A wide wavelength range optical switch using a flexible photonic crystal waveguide and silicon rods *J. Micromech. Microeng.* **20** 075009

[16] Abdulla S M C, Kauppinen L J, Dijkstra M, Berenschot E, de Boer M J, de Ridder R M and Krijnen G J M 2011 Mechano-optical switching in a MEMS integrated photonic crystal slab waveguide *IEEE 24th Int. Conf. on Micro Electro Mechanical Systems* pp 9–12

[17] Suh W, Yanik M F, Solgaard O and Fan S 2003 Displacement-sensitive photonic crystal structures based on guided resonance in photonic crystal slabs *Appl. Phys. Lett.* **82** 1999–2001

[18] Suh W and Fan S 2003 Mechanically switchable photonic crystal filter with either all-pass transmission or flat-top reflection characteristics *Opt. Lett.* **28** 1763–5

[19] Park W and Lee J B 2004 Mechanically tunable photonic crystal structure *Appl. Phys. Lett.* **85** 4845–7

[20] Zhou W, Mackie D M, Taysing-Lara M, Dang G, Newman P G and Svensson S 2006 Novel reconfigurable semiconductor photonic crystal-MEMS device *Solid-State Electron.* **50** 908–13

[21] Takahata T, Hoshino K, Matsumoto K and Shimoyama I 2006 Transmittance tuning of photonic crystal reflectors using an SPM cantilever *Sensors Actuators* A **128** 197–201

[22] Marki I, Salt M and Herzig H P 2006 Tuning the resonance of a photonic crystal microcavity with an AFM probe *Opt. Express* **14** 2969–78

[23] Cluzell B, Lalouat L, Velha P, Picard E, Peyrade D, Rodier J C, Charvolin T, Lalanne P, de Fornel F and Hadji E 2008 A near-field actuated optical nanocavity *Opt. Express* **16** 279–86

[24] Blaber M G, Arnold M D and Ford M J 2009 Search for the ideal plasmonic nanoshell: the effects of surface scattering and alternatives to gold and silver *J. Phys. Chem.* C **113** 3041–5

[25] Beams J W 1959 *Structure and Properties of Thin Films* (New York: Wiley)

[26] Shackelford J F and Alexander W 2000 *CRC Materials Science and Engineering Handbook* (Boca Raton, FL: CRC Press)

[27] Oskooi A F, Roundy D, Ibanescu M, Bermel P, Joannopoulos J D and Johnson S G 2010 Meep: a flexible free-software package for electromagnetic simulations by the FDTD method *Comput. Phys. Commun.* **181** 687–702

[28] Mandelshtam V A and Taylor H S 1997 Harmonic inversion of time signals *J. Chem. Phys.* **107** 6756–69

[29] Yang J, Ono T and Esashi M 2001 Investigating surface stress: surface loss in ultrathin single-crystal silicon cantilevers *J. Vac. Sci. Technol.* B **19** 551–6

[30] Fu X A, Jezeski R, Zorman C A and Mehregany M 2004 Use of deposition pressure to control residual stress in polycrystalline SiC films *Appl. Phys. Lett.* **84** 341–3

[31] Fritz J, Baller M K, Lang H P, Rothuizen H, Vettiger P, Meyer E, Güntherodt H J, Gerber C and Gimzewski J K 2000 Translating biomolecular recognition into nanomechanics *Science* **288** 316–8

[32] Zhang J, Lang H P, Huber F, Bietsch A, Grange W, Certa U, McKendry R, Güntherodt H J, Hegner M and Gerber C 2006 Rapid and label-free nanomechanical detection of biomarker transcripts in human RNA *Nature Nanotechnol.* **1** 214–20

[33] Rasmussen P A, Thaysen J, Hansen O, Eriksen S C and Boisen A 2003 Optimised cantilever biosensor with piezoresistive read-out *Ultramicroscopy* **97** 371–6

[34] Bahreynia B, Najafib F and Shafaia C 2006 Piezoresistive sensing with twin-beam structures in standard MEMS foundry processes *Sensors Actuators* A **127** 325–31

[35] Li M, Pernice W H P and Tang H 2009 Broadband all-photonic transduction of nanocantilevers *Nature Nanotechnol.* **4** 377–82

[36] Lin Q, Rosenberg J, Chang D, Camacho R, Eichenfield M, Vahala K J and Painter O 2010 Coherent mixing of mechanical excitations in nano-optomechanical structures *Nature Photon.* **4** 236–42